$CuNNi_3$: a new nitride superconductor with antiperovskite structure

OPEN ACCESS
IOP PUBLISHING
SUPERCONDUCTOR SCIENCE AND TECHNOLOGY
Supercond. Sci. Technol. **26** (2013) 125015 (6pp)
doi:10.1088/0953-2048/26/12/125015

$CuNNi_3$: a new nitride superconductor with antiperovskite structure

Bing He[1,2], Cheng Dong[1], Lihong Yang[1], Xiaochao Chen[1], Linhui Ge[1], Libin Mu[1] and Youguo Shi[1]

[1] Institute of Physics, Chinese Academy of Science, Beijing 100190, People's Republic of China
[2] Luzhou Medical College, Luzhou, Sichuan 646000, People's Republic of China

E-mail: hebing_wu@163.com

Received 23 July 2013, in final form 24 September 2013
Published 4 November 2013
Online at stacks.iop.org/SUST/26/125015

Abstract
We have successfully synthesized a new Ni-based antiperovskite nitride, $CuNNi_3$, which exhibits superconductivity with a transition temperature T_c of 3.2 K. This compound is the second nitride superconductor in the Ni-based antiperovskites. We report the synthesis and physical properties of $CuNNi_3$, characterized via x-ray diffraction, magnetization, resistivity, and heat capacity measurements. The temperature dependence of the specific heat is consistent with an isotropic s-wave gap ($\Delta_0 = 0.42$ meV). The estimated electron–phonon coupling strength ($\lambda_{ep} = 0.53$) suggests that the superconductivity in $CuNNi_3$ is induced by electron–phonon coupling, and the gap ratio ($2\Delta_0/k_BT_c$) of 3.05 indicates that it is a weak coupling superconductor. Furthermore, the relatively high Ginzburg–Landau parameter ($\kappa = 24.6$) signifies that $CuNNi_3$ is a type II superconductor.

(Some figures may appear in colour only in the online journal)

1. Introduction

Since the superconductivity of $MgCNi_3$ was discovered [1], many experimental and theoretical studies have been made to find new superconductors among the antiperovskite compounds $MXNi_3$, where M is mostly a divalent or trivalent metal and X is C or N. Among the $MCNi_3$ (M = Cd, Zn, Al, Ga, In) carbide antiperovskites [2–6], only $CdCNi_3$ demonstrates superconductivity with a T_c of 3.4 K. Recently, several new nitride antiperovskites, $MNNi_3$ (M = Zn, In, Cd), have been synthesized [7–11], and superconductivity with a T_c of 3 K was found in $ZnNNi_3$. Both $InNNi_3$ and $CdNNi_3$ exhibit metallic behavior and show no superconductivity down to 2 K [10, 11].

The discovery of superconductivity in $ZnNNi_3$ has led us to study other nitride antiperovskites, $MNNi_3$. The mechanical and electronic properties of $MNNi_3$ (M = Zn, Mg, Cd, Al, Ga, In, Sn, Sb, Pd, Cu, Ag, Pt) have been studied using various theoretical methods [12–22]. First principle band calculations for $ZnNNi_3$ revealed that a large and narrow peak of mainly Ni 3d character is located just below the Fermi energy (E_F) in the density of states (DOS) curves [12, 13, 21]. According to the rigid band approximation, hole doping in $ZnNNi_3$ could increase the density of states at the Fermi level. If we consider $CuNNi_3$ as a hole doped $ZnNNi_3$, the E_F of $CuNNi_3$ should be located closer to the Ni 3d peak, i.e., in the region of quite high DOS, which is favorable for superconductivity. Helal and Islam studied the elastic, electronic, and optical properties of $MNNi_3$ (M = Zn, Sn, and Cu) by first-principle calculations in 2011 [21]. They found that the electronic band structures of $SnNNi_3$ and $CuNNi_3$, two 'hypothetical' compounds at that time, show metallic behavior just like the superconducting $ZnNNi_3$, and expected that their calculations would motivate experimental study on $SnNNi_3$ and $CuNNi_3$. There is no information in the current literature concerning the preparation and superconductivity of $CuNNi_3$.

In this paper we report the synthesis, crystal structure and superconducting and normal-state properties of $CuNNi_3$. From the experimental data, we determined the lower

critical field $H_{c1}(0)$, upper critical field $H_{c2}(0)$, coherence length $\xi(0)$, penetration depth $\lambda(0)$, Ginzburg–Landau (GL) parameter $\kappa(0)$, electronic specific-heat coefficient γ and Debye temperature Θ_D for $CuNNi_3$.

2. Experimental details

Polycrystalline samples of $CuNNi_3$ were synthesized by solid–gas reactions. Stoichiometric Cu (99.7%) and Ni (99.8%) powders were mixed and ground thoroughly. The mixture was heated in a tube furnace at 673 K for 3 h in flowing NH_3 (99.9%, 80 ml min^{-1}). The as-prepared powders were thoroughly reground, pelletized, initially sintered at 773 K for 6 h and finally sintered at 833 K for 6 h in flowing NH_3. The powder x-ray diffraction (PXRD) data of the sample were collected on an MXP18A-HF diffractometer with Cu Kα radiation. The Rietveld refinement of the diffraction data was performed using the program RIETAN-2000 [23]. The chemical composition of the sample was analyzed by an energy dispersive x-ray spectrometer (EDXS) attached to a scanning electron microscope (XL30 S-FEG). Additionally, an elemental analyzer (Elementary Vario Micro Cube) was used to analyze the nitrogen content. Magnetic measurements were performed in a superconducting quantum interference device magnetometer (MPMS XL-7, Quantum Design). The resistivity and specific heat were measured on a physical properties measurement system (PPMS, Quantum Design) with a dilution refrigerator. All $M(H)$ curves were taken in the zero-field-cooled (ZFC) mode with initial temperature up to 6 K. A low-field sweep rate of 20 Oe min^{-1} was selected to measure isothermal magnetization curves.

3. Results and discussion

Our $CuNNi_3$ sample is a stoichiometric compound based on the results of the EDX analysis, elemental analysis and the Rietveld refinement of the PXRD data. EDX analysis revealed that the actual Cu/Ni atomic ratio is consistent with the nominal composition ($CuNNi_3$) within the experimental error. The elemental analysis showed that the weight percentage of nitrogen is 5.5%. This result corresponds to $y = 0.99$ in CuN_yNi_3. The diffraction peaks could be indexed well with a cubic antiperovskite unit cell. Using the antiperovskite structure as a starting model, the lattice parameter and the occupancy of the nitrogen atom were refined using the Rietveld method. The occupancy of the nitrogen atom was refined together with other structural parameters. The Rietveld refinement pattern for $CuNNi_3$ is shown in figure 1. The refined structural parameters and R factors are listed in table 1. The occupancy of the nitrogen atom is refined to 1.008(3), which agrees well with the result obtained by elemental analysis. The lattice parameter a is refined to be 3.742(2) Å, which agrees quite well with the data ($a = 3.745$ Å) predicted by first-principle calculations [14].

The temperature dependence of the electrical resistivity of $CuNNi_3$ is shown in figure 2(a). The curve shows good metallic behavior with a residual resistivity (ρ_0) of 15 $\mu\Omega$ cm. From the inset of figure 2(a), it can be seen that the resistivity

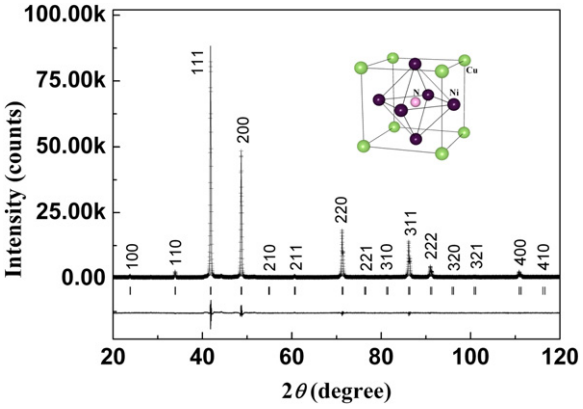

Figure 1. The Rietveld refinement pattern for $CuNNi_3$. The crosses (+) correspond to the experimental data. The solid line represents the calculated pattern. The short vertical lines mark the positions of allowed reflections. The curve at the bottom of the plot gives the difference between the experimental and calculated patterns. The inset shows the crystal structure of $CuNNi_3$.

Table 1. Refined structural parameters for $CuNNi_3$.

Atom	Site	x	y	z	B (Å^2)	Occupancy
Cu	1a	0	0	0	0.97(6)	1.0
N	1b	0.5	0.5	0.5	1.2(4)	1.008(3)
Ni	3c	0	0.5	0.5	1.09(2)	1.0

$R_p = 6.94\%$, $R_{wp} = 8.95\%$, $R_{ex} = 4.86\%$,
$a = 3.742(2)$ Å

drops sharply to zero at 3.2 K. Figure 2(b) presents the dc susceptibility measurements under 20 Oe magnetic field. It is found that a sharp diamagnetic transition occurs at 3.2 K and the diamagnetic value approaches a constant at 2.8 K. Compared with the zero-field-cooled (ZFC) data, the much lower field-cooled (FC) diamagnetic signal is an indication of a substantial pinning effect, possibly on grain boundaries. Thus the susceptibility and resistivity give a self-consistent $T_c = 3.2$ K for $CuNNi_3$. The transition width and residual resistivity ratio (RRR) were 0.4 K and 19, respectively, indicating high quality and homogeneity of the sample.

Figure 3 shows the specific heat divided by the temperature (C/T) as a function of T^2 under different magnetic fields from 0 to 1 T. The bulk nature of the superconductivity and the good quality of the sample are confirmed by a sharp anomaly at 3.2 K under $H = 0$, which is consistent with the T_c determined by the susceptibility and resistivity data. Regarding the relatively low T_c of the sample, the normal-state specific heat could be extracted easily with the simple relation $C/T = \gamma_n + \beta T^2$, where the first and the second terms correspond to the electronic and phonon contributions, respectively. The solid line in figure 3 shows the curve fitted by the formula $C/T = \gamma_n + \beta T^2$. From this fitting, γ_n and β are estimated to be 39.27 mJ (mol $K^2)^{-1}$ and 0.392 mJ (mol $K^4)^{-1}$, respectively. By extrapolating the low temperature data for zero field down to 0 K, a small residual value $\gamma_0 = 0.75$ mJ (mol $K^2)^{-1}$ is obtained, indicating a small non-superconducting volume fraction of

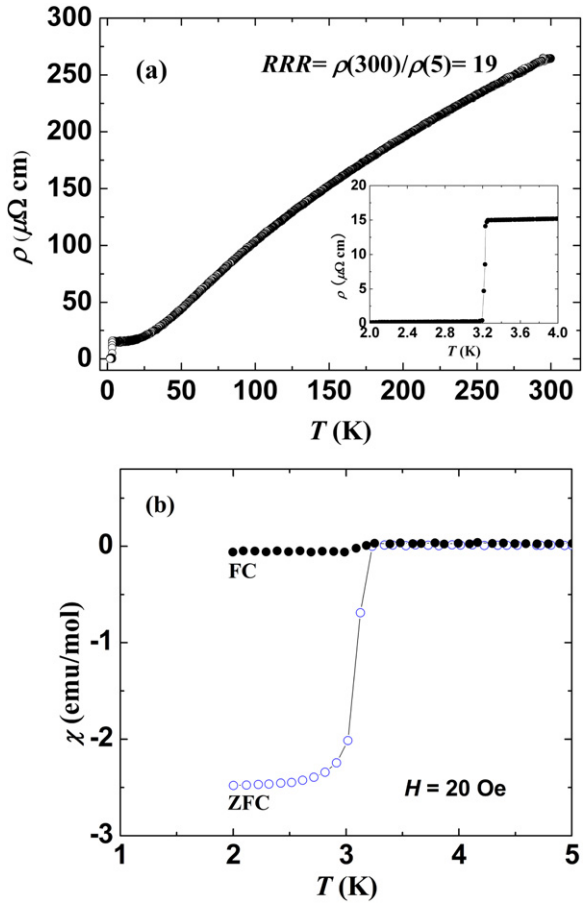

Figure 2. (a) The resistivity as a function of temperature for $CuNNi_3$ up to room temperature. The inset shows an enlarged portion in the superconducting transition region. (b) The temperature dependence of the susceptibility χ at $H = 20$ Oe under zero-field-cooled (ZFC) and field-cooled (FC) conditions.

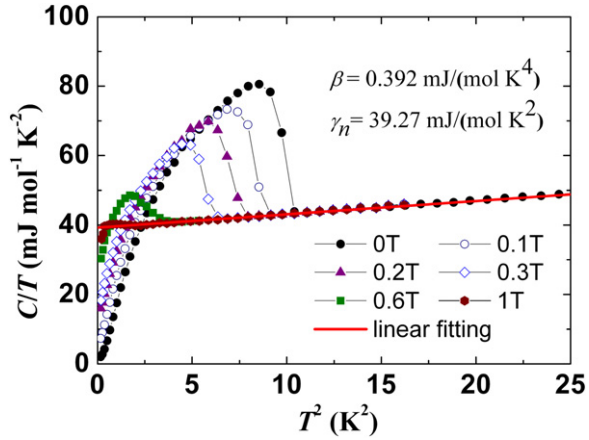

Figure 3. The specific heat of $CuNNi_3$ plotted as C/T versus T^2 under various magnetic fields. The solid line shows a fit using the formula $C/T = \gamma_n + \beta T^2$.

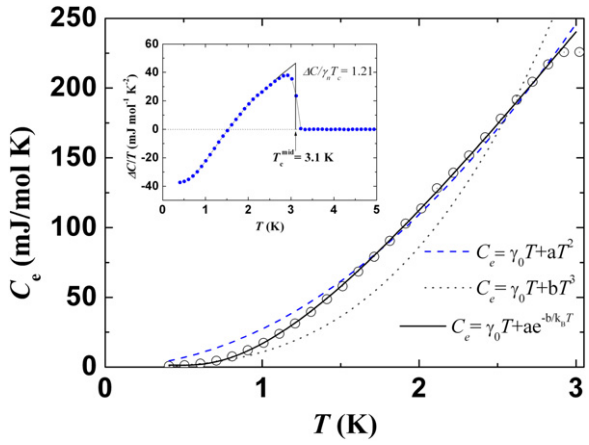

Figure 4. Electronic specific-heat data C_e versus T in the superconducting state (circles). The lines are fits described in the text. The inset shows $\Delta C/T$ versus T. Dotted line: entropy conserving construction to get the idealized jump.

about 2%. The normal state Sommerfeld constant for the present sample could be determined from the relation $\gamma_e = \gamma_n - \gamma_0$, yielding 38.52 mJ (mol K^2)$^{-1}$. It is noticeable that the value of γ_n determined in our measurement is higher than that of $ZnNNi_3$ [7], indicating the higher density of states in $CuNNi_3$. Using the relation $\Theta_D = (\frac{12\pi^4}{5\beta}nR)^{1/3}$, where $R = 8.314$ J (mol K)$^{-1}$ and $n = 5$ is the number of atoms in one unit cell, we get the Debye temperature $\Theta_D = 291$ K. The electron–phonon coupling constant (λ_{ep}) can be estimated from the McMillan formula [24]

$$T_c = \frac{\Theta_D}{1.45}\exp\left[-\frac{1.04(1+\lambda_{ep})}{\lambda_{ep}-\mu^*(1+0.62\lambda_{ep})}\right], \qquad (1)$$

where μ^* is the Coulomb pseudopotential taking a value of about 0.11. Using $\Theta_D = 291$ K and $T_c = 3.2$ K, we obtain $\lambda_{ep} = 0.53$. Therefore, we can say that $CuNNi_3$ is a weak coupling superconductor.

Figure 4 shows the electronic specific heat (C_e) below T_c, obtained from the zero field data. Three models were used to fit the data, $C \propto T^2$, T^3, and $e^{-b/kT}$, expected for line nodes, point nodes, and a fully gapped model, respectively. The small residual linear term $\gamma_0 T$ of 0.75 T (mJ mol^{-1} K^{-1}) was held constant throughout the fits. The best fit is provided by a fully gapped model. An s-wave BCS model of the entire C_e data gives an isotropic gap value $\Delta_0 = 0.42$ meV. The ratio $2\Delta_0/k_BT_c = 3.05$ obtained here is close to the prediction for the weak coupling limit ($2\Delta_0/k_BT_c = 3.53$), indicating a weak coupling strength. The inset of figure 4 shows the superconducting part of the electronic specific heat $\Delta C(T) = C(T) - \beta T^3 - \gamma_n T$, obtained from the zero field data. The superconducting transition temperature $T_c = 3.1$ K has been estimated by an entropy conserving construction (solid line in the inset of figure 4). This value agrees well with the transition temperature $T_c = 3.2$ K derived from resistivity and dc susceptibility data. The normalized specific heat jump at $T_c = 3.1$ K is $\Delta C/\gamma_n T_c = 1.21$. This is close to the BCS value (1.43), indicating that $CuNNi_3$ is a weak electron–phonon coupling superconductor.

Dominance of an s-wave channel is supported by measurements of the magnetic field dependence of the Sommerfeld parameter $\gamma_e(H)$ [25]. It is known that the electronic specific heat in a magnetic field can be expressed

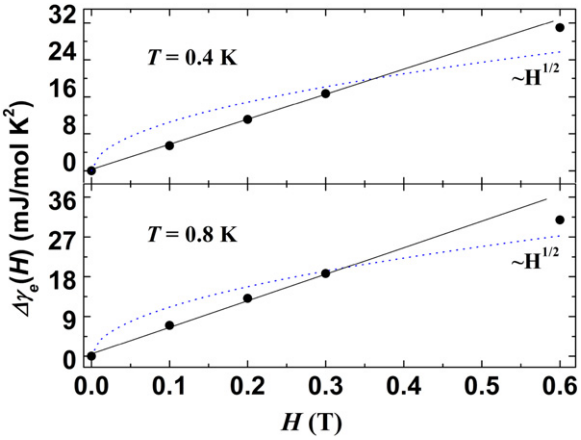

Figure 5. The magnetic field dependence of $\Delta\gamma_e$ as a function of the magnetic field H below 0.6 T. The solid line corresponds to a linear ($\sim H$) relation and the dotted line represents the nonlinear ($\sim H^{1/2}$) relation.

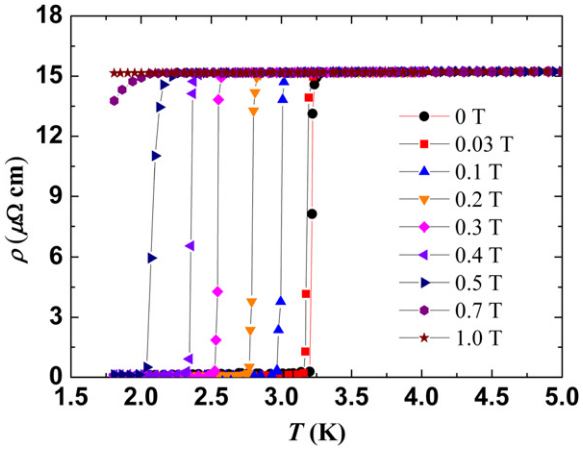

Figure 6. The temperature dependence of the resistivity under different dc magnetic fields.

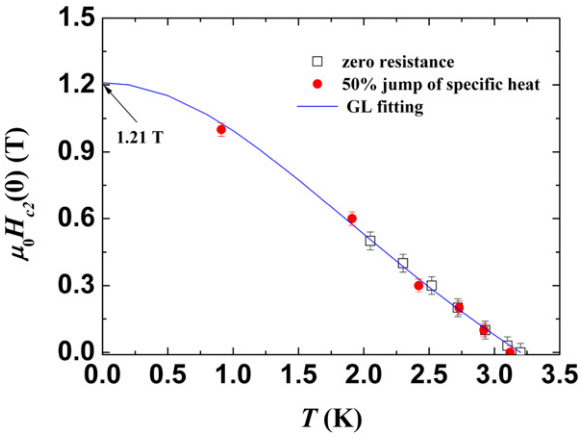

Figure 7. The temperature dependence of the upper critical field obtained by resistivity (open squares) and specific-heat (red circles) measurements. The solid line is a fit of the Ginzburg–Landau (GL) formula.

by $C_e(T, H) = C_e(T,\ H = 0) + \gamma_e(H)T$. The magnetic field dependence of $\gamma_e(H)$ is associated with the form of the gap function of the superconductor. For a highly anisotropic gap or a gap with nodes, $\gamma_e(H) \propto H^{1/2}$ is predicted [26]. In contrast, for a fully gapped superconductor, $\gamma_e(H)$ is expected to be proportional to H [27]. Figure 5 shows the magnetic field dependence of $\Delta\gamma_e = \gamma_e(H) - \gamma_e(0)$ as function of the magnetic field H at $T = 0.4$ and 0.8 K. As shown in figure 5, the field-linear increase in $\Delta\gamma_e(H)$ suggests that most electronic states near the Fermi energy are gapped in $CuNNi_3$ and clearly is at odds with a $\Delta\gamma_e(H) \propto H^{1/2}$ dependence. This linear relation is demonstrated well by the data below 0.6 T, providing more evidence for the s-wave pairing.

Figure 6 shows the temperature dependence of the resistivity under different magnetic fields. It is observed that the superconductivity (onset transition point) is depressed completely at about 1 T above 1.8 K. Using the criterion of zero resistivity and 50% jump of the specific-heat anomaly, we obtained the upper critical field $\mu_0 H_{c2}$ for $CuNNi_3$ (see figure 7). As shown in figure 7, the upper critical fields obtained from resistivity and specific-heat measurements coincide with each other within the experimental uncertainty. The upper critical field $\mu_0 H_{c2}(0)$ can be estimated by the Werthamer–Helfand–Hohenberg (WHH) relation for a BCS superconductor with weak coupling [28],

$$\mu_0 H_{c2} = -0.693(\mathrm{d}H_{c2}/\mathrm{d}T_c)T_c, \tag{2}$$

where the slope $\mathrm{d}H_{c2}/\mathrm{d}T_c = -0.51$ T K^{-1}. For $T_c = 3.2$ K, $\mu_0 H_{c2}(0)$ was found to be 1.13 T. Ginzburg–Landau theory provides an alternative estimate for the upper critical field, where $\mu_0 H_{c2}(0)$ can be determined from the simple empirical formula [29]

$$\mu_0 H_{c2}(T) = \mu_0 H_{c2}(0)\frac{1 - t^2}{1 + t^2}, \tag{3}$$

where t is the normalized temperature T/T_c and $\mu_0 H_{c2}(0)$ is the upper critical field extrapolated to 0 K. The solid line in figure 7 shows the best fit of resistivity data by equation (3). The extrapolation yielded $\mu_0 H_{c2}(0) = 1.21$ T, which is close to the WHH estimate.

The low critical field values, $\mu_0 H_{c1}(T)$, were determined from the low-field magnetization curves. The inset of figure 8 shows the initial part of the magnetization curves over the temperature range from 2.0 to 3.0 K. The low-field parts of these magnetization curves almost overlap on a common Meissner line (as shown by a solid line in figure 8) due to the Meissner effect. Therefore, $\mu_0 H_{c1}(T)$ could be determined at the point where the magnetization curve starts to deviate from the 'Meissner line'. Figure 8 shows the temperature dependence of $\mu_0 H_{c1}(T)$. The data for $\mu_0 H_{c1}(T)$ could be fitted with the empirical formula $\mu_0 H_{c1}(T) = \mu_0 H_{c1}(0)[1 - (T/T_c)^2]$ [29] and $\mu_0 H_{c1}(0)$ was determined to be 4.0 mT.

With these results for $\mu_0 H_{c1}(0)$ and $\mu_0 H_{c2}(0)$, we can estimate several superconducting parameters for $CuNNi_3$. The superconducting coherence length $\xi(0)$ and penetration depth $\lambda(0)$ can be estimated by using the relations $\xi(0) = [\phi_0/2\pi H_{c2}(0)]^{1/2}$ and $\lambda(0) = [\phi_0/2\pi H_{c1}(0)]^{1/2}$, where ϕ_0 is the quantum of flux. The values of $\xi(0)$ and $\lambda(0)$ come out to be 165 Å and 4058 Å, respectively. Consequently, the

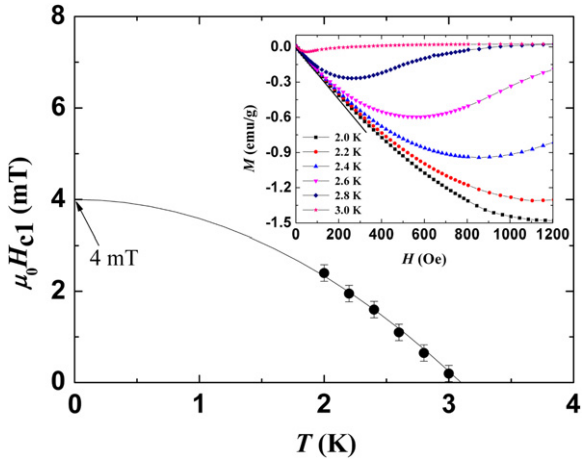

Figure 8. The temperature dependence of $\mu_0 H_{c1}$. The inset shows magnetization curves at several temperatures used for determining H_{c1}.

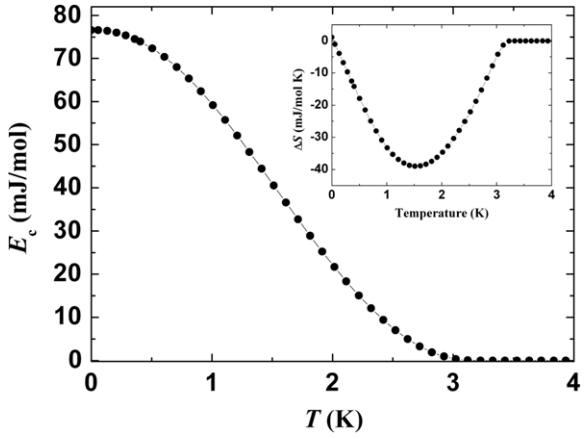

Figure 9. Superconducting condensation energy E_c of $CuNNi_3$ calculated by using specific-heat data. The inset shows the entropy difference between the normal and the superconducting states.

Ginzburg–Landau parameter $\kappa = \lambda(0)/\xi(0)$ is 24.6, showing that this system is a type II superconductor. Using these parameters, the thermodynamic critical field $\mu_0 H_c(0)$ could be obtained from the following relation [25]:

$$H_{c1} H_{c2} = H_c^2(0) \ln \kappa. \tag{4}$$

We find that the thermodynamic critical field $\mu_0 H_c(0) =$ 38.9 mT.

The superconducting condensation energy (E_c) provides a stringent self-consistency check on the derived parameters [25]. Therefore, we calculate E_c with the specific-heat data as follows. The entropy difference between the normal state and the superconducting state is obtained by $\Delta S(T) = \int_0^T (\Delta C/T)\, dT'$, and E_c is determined through $E_c = \int_T^{4K} \Delta S(T)\, dT'$. Figure 9 shows the temperature dependence of the condensation energy E_c, which is about 76.6 mJ mol^{-1} at 0 K. The inset shows the entropy difference between the normal state and the superconducting state. Actually, E_c can also be calculated by the following equation [30]:

$$E_c = \alpha N(E_F) \Delta_0^2/2 = \alpha \frac{3}{4\pi^2} \frac{1}{k_B^2} \gamma_n \Delta_0^2. \tag{5}$$

For a BCS s-wave superconductor, $\alpha = 1$, using $\gamma_n =$ 38.52 mJ (mol K^2)$^{-1}$ and $\Delta_0 = 0.42$ meV, we obtain a value of $E_c = 71.1$ mJ mol^{-1}, which is close to the value of 76.6 mJ mol^{-1} obtained above. The consistency between the E_c values obtained by two different methods verifies the validity of the determined γ_n and Δ_0. The thermodynamic critical field $\mu_0 H_c(0)$ can also be obtained by the relation $\mu_0 H_c^2(0)/2 = F_N - F_S = \int\int (\Delta C/T)\, dT$. This gives the value of $\mu_0 H_c(0)$ as 38.7 mT, which is in excellent agreement with that derived from the critical fields. Table 2 summarizes the superconducting- and normal-state parameters that we obtained for $CuNNi_3$ and, for comparison, those of $ZnNNi_3$ [7] are also shown.

Table 2. Superconducting- and normal-state properties for $CuNNi_3$ and $ZnNNi_3$.

Parameter	$ZnNNi_3$	$CuNNi_3$
T_c (K)	3.0	3.2
$\mu_0 H_{c1}(0)$ (mT)	6.9	4.0
$\mu_0 H_{c2}(0)$ (T)	0.96	1.21
$\mu_0 H_c(0)$ (mT)	—	38.7
$\xi(0)$ (Å)	185	165
$\lambda(0)$ (Å)	3089	4058
$\kappa(0)$	17	24.6
$2\Delta(0)/k_B T_c$	—	3.05
$\Delta C/\gamma_n T_c$	—	1.21
γ (mJ (mol K^2)$^{-1}$)	13	39.27
β (mJ (mol K^4)$^{-1}$)	0.26	0.392
Θ_D (K)	336	291

4. Conclusion

In summary, we succeeded in synthesizing a new nitride superconductor, $CuNNi_3$, with antiperovskite structure. The nitrogen content in the $CuNNi_3$ sample was determined to be close to stoichiometric by elemental analysis and Rietveld refinement. The superconducting- and normal-state properties of $CuNNi_3$ were determined by means of magnetic susceptibility, electrical resistivity, and specific-heat measurements. An analysis of the temperature dependence of the specific heat shows that the superconducting properties are dominated by an isotropic s-wave gap with value $\Delta_0 =$ 0.42 meV, and $CuNNi_3$ could be categorized as a type II superconductor with weak electron–phonon coupling.

It seems rather puzzling that complete substitution of Zn by Cu in $ZnNNi_3$ generates a new superconductor $CuNNi_3$ with almost the same T_c because Cu and Zn have distinctly different electronic structures. It is well known that Zn doping can seriously suppress or even destroy the superconductivity in cuprates. Therefore, theoretical calculations are greatly desired to interpret the superconductivity of $CuNNi_3$. Although the structural, elastic, electronic, and optical properties of $CuNNi_3$ have been investigated using first-principle calculations [21], no theoretical calculation results

on the superconductivity of $CuNNi_3$ have been reported. Recently, some theorists in our institute have studied the superconducting properties of $CuNNi_3$ using first-principle calculations, and obtained a superconducting transition temperature which is close to our experimental value. Their research results will be published soon.

Acknowledgments

This work was supported by the National Natural Science Foundation of China (No. 20871119), the National Basic Research Program of China (973 Program) 2011CBA00100 and 2011CB808202, and the Natural Science Foundation of Sichuan Education Department 132ZA0234.

References

[1] He T, Huang Q, Ramirez A P, Wang Y, Regan K A, Rogado N, Hayward M A, Haas M K, Slusky J S and Inumara K 2001 *Nature* **411** 54
[2] Uehara M, Yamazaki T, Kroi T, Kashida T, Kimishima Y and Ohishi K 2007 *J. Phys. Chem. Solids* **68** 2178
[3] Uehara M, Amano T, Takano S, Kôri T, Yamazaki T and Kimishima Y 2006 *Physica* C **440** 6
[4] Dong A F, Che G C, Huang W W, Jia S L, Chen H and Zhao Z X 2005 *Physica* C **422** 65
[5] Tong P, Sun Y P, Zhu X B and Song W H 2007 *Solid State Commun.* **141** 336
[6] Tong P, Sun Y P, Zhu X B and Song W H 2006 *Phys. Rev.* B **73** 245106
[7] Uehara M, Uehara A, Kozawa K and Kimishima Y 2009 *J. Phys. Soc. Japan* **78** 033702
[8] Karki A B, Xiong Y M, Young D P and Adams P W 2009 *Phys. Rev.* B **79** 212508
[9] Cao W H, He B, Liao C Z, Yang L H, Zeng L M and Dong C 2009 *J. Solid State Chem.* **182** 3353
[10] Uehara M, Uehara A, Kozawa K and Kimishima Y 2010 *Physica* C **470** S688
[11] He B, Dong C, Yang L H, Ge L H and Chen H 2011 *J. Solid State Chem.* **184** 1939
[12] Shein I R, Bannikov V V and Lvanovskii A L 2010 *Phys. Status Solidi* b **247** 72
[13] Okoye C M I 2010 *Physica* B **405** 1562
[14] Bannikov V V, Shein I R and Ivanovskii A L 2010 *Physica* B **405** 4615
[15] Li C, Chen W G, Wang F, Li S F, Sun Q, Wang S and Jia Y 2009 *J. Appl. Phys.* **105** 123921
[16] Shim J H, Kwon S K and Min B I 2001 *Phys. Rev.* B **64** 180510
[17] Tütüncü M and Srivastava G P 2006 *J. Phys.: Condens. Matter* **18** 11089
[18] Bannikov V V, Shein I R and Ivanovskii A L 2010 *Comput. Mater. Sci.* **49** 457
[19] Hou Z F 2010 *Solid State Commun.* **150** 1874
[20] Alexandrov K S and Beznosikov B V 2004 *Perovskites: Present and Future* (Novosibirsk: Perseus Books) pp 200–1 (in Russian)
[21] Helal M A and Islam A K 2011 *Physica* B **406** 4564
[22] Ali M A, Islam A K and Ali M S 2012 *J. Sci. Res.* **4** 1
[23] Izumi F and Ikeda T 2000 *Mater. Sci. Forum* **189** 321
[24] McMillan W L 1968 *Phys. Rev.* **167** 331
[25] Klimczuk T, Ronning F, Sidorov V, Cava R J and Thompson J D 2007 *Phys. Rev. Lett.* **99** 257004
[26] Volovik G E 1993 *JETP Lett.* **58** 469
[27] Caroli C, Gennes P G and Matricon J 1964 *Phys. Lett.* **9** 307
[28] Werthamer N R, Helfand E and Hohenberg P C 1966 *Phys. Rev.* **147** 295
[29] Carbotte J P 1990 *Rev. Mod. Phys.* **62** 1027
[30] Schrieffer J R 1999 *Theory of Superconductivity* (Perseus Books)